Direct observation of electric field induced pattern formation and particle aggregation in ferrofluids

Michal Rajnak,[a] Viktor I. Petrenko,[b,c] Mikhail V. Avdeev,[b] Olexandr I. Ivankov,[b,c,f] Artem Feoktystov,[d] Bystrik Dolnik,[e] Juraj Kurimsky,[e] Peter Kopcansky,[a] Milan Timko[a]

[a]Institute of Experimental Physics SAS, Watsonova 47, 04001 Košice, Slovakia

[b]Joint Institute for Nuclear Research, Joliot-Curie 6, 141980 Dubna, Moscow region, Russia

[c]Kyiv Taras Shevchenko National University, Volodymyrska Street 64, Kyiv, 01033 Ukraine

[d]Jülich Centre for Neutron Science (JCNS), Forschungszentrum Jülich GmbH, Outstation at MLZ, Lichtenbergstrasse 1, 85747 Garching, Germany

[e]Faculty of Electrical Engineering and Informatics, Technical University of Košice, Letná 9, 04200 Košice, Slovakia

[f]Moscow Institute of Physics and Technology, Institutskiy per. 9, Dolgoprudniy, 141700, Russia

KEYWORDS: ferrofluid, magnetic nanoparticles, pattern formation, aggregation, electric field

ABSTRACT

Ferrofluids typically respond to magnetic fields and can be manipulated by external magnetic fields. Here we report on formation of visually observable patterns in a diluted low-polarity ferrofluid exposed to external electric fields. This presents a specific type of ferrofluid structure driven by a combined effect of electrohydrodynamics and electrical body forces. The free charge and permittivity variation are considered to play a key role in the observed phenomenon. The corresponding changes in the ferrofluid structure have been found at nanoscale as well. By

small-angle neutron scattering (SANS) we show that the magnetic nanoparticles aggregate in direct current (dc) electric field with a strong dependence on the field intensity. The anisotropic aggregates preferably orient in the direction of the applied electric field. Conducting SANS experiments with alternating current (ac) electric fields of various frequencies we found a critical frequency triggering the aggregation process. Our experimental study could open future applications of ferrofluids based on insulating liquids.

TEXT:

Ferrofluids are remarkable suspensions of magnetic nanoparticles (MNPs) in conventional base fluids such as water, oils, or glycols.[1] With recent advances in MNPs synthesis and a rich history grounded colloidal science, ferrofluids have recently been engineered for a rapidly increasing number of applications.[2,3] In most cases, enhanced magnetic, rheological and thermal properties of the base fluids containing MNPs are primarily due to the interaction of their magnetic moments with a magnetic field. This interaction and the subsequent structural particle reorganization (chains, aggregates, and pattern formation) have been intensively studied by various experimental methods and theoretical approaches.[4–10] As the formation of colloidal patterns has many potential uses in materials processing, the structures of MNPs formed in magnetic fields are crucial in the ferrofluid research. Analogously, structural transitions in various colloidal suspensions can be induced by electric fields leading to particle-particle electrostatic interactions, playing an important role in numerous self-assembly phenomena.[11–15] However, similar response of ferrofluids to electric fields has not been directly observed yet.

Investigation of dielectric properties of ferrofluids is especially desirable when a ferrofluid

is intended for high voltage engineering purposes. MNPs in transformer oils enhance the cooling effect (thermo-magnetic convection), and increase the dielectric breakdown field strength of transformer oils.[16–18] While the former effect is fairly intuitive, the latter is paradoxical and still not fully understood. It is known that polarization of MNPs increases the relative permittivity of ferrofluids.[19] However, particle-particle interactions due to their polarization and potential electric field induced aggregation have not been sufficiently investigated yet. Recently, dielectric spectroscopy studies on thin layers of transformer oil-based ferrofluids (TOFF) revealed strong indications that the external electric field induces MNPs aggregation.[20,21] Such a response of MNPs to electric fields may affect the breakdown field strength of TOFF, especially in regard to the theory of converting free electrons to charged particles forming a streamer.[22,23]

In this letter we present the formation of visually observable patterns in a TOFF exposed to an electric field. The effect is accompanied by a specific particle aggregation, as concluded from SANS experiments. The TOFF sample consists of magnetite nanoparticles dispersed in transformer oil with the relative permittivity of 2.1. The nanoparticles were coprecipitated from aqueous solution of Fe^{2+} and Fe^{3+}, and stabilized by oleic acid in a well proven way.[24,25] Two samples[21] with the magnetic volume fraction of 0.05 % (visual observation) and 1 % (SANS and electric current measurements) were studied. For all the reported experiments we used a standard quartz cuvette (Hellma, 1 mm thick) equipped with two stainless tubular electrodes inside, fixed 1 cm apart in the Teflon stoppers (Fig. 1a). Our simulation confirmed a homogenous field in the middle of the cuvette, while the near electrode regions exhibit gradient field with the strongest intensity in the stoppers. *In situ* SANS experiments were carried out on the small-angle neutron diffractometers including the time-of-flight YuMO instrument[26] at the pulsed IBR-2 reactor at JINR, Dubna, Russia, and the KWS-1 instrument[27] at the steady-state FRM-II reactor at MLZ,

Garching, Germany. The obtained SANS curves coincide in the overlapping scattering vector range of the two instruments. The experiments were performed at room temperature with the sample aperture of 8x8 mm^2 centered in the middle between the electrodes.

The first solid evidence of the electric field and the consequent electrohydrodynamics influence on the TOFF is presented in Figure 1, which illustrates the sample exposed to 5 kV/cm (dc). A few seconds after applying the electric field, the particle concentration around the electrodes started to decrease visibly at the expense of the shady cloud formation between the electrodes. A final shade of the cloud had been achieved in approximately 2 minutes (Fig. 1b), and spike-like edges started to grow from the cloud borders pointing towards the electrodes (Fig. 1c-j). One can see the slow dynamics as the spikes vary in length, width, and position. The initial clearing effect is associated with the migration of the space charges (including residual unwashed ions) towards the electrodes, which engenders weak fluid flow. As the ions accumulate in the field gradient onto the electrodes, the particles are pushed from that region, leading to the cloud-like formation. The sample with the separated cloud exhibits the permittivity and conductivity gradients, and the further action of the dc field exerts an anisotropic electrostatic body force on the transition layer between the cloud and its surrounding. This force sets the cloud in motion and distorts its shape in the direction of the applied field. The distortion begins in the upper part and the spikes direct rather upwards, not horizontally, due to the strong field gradient in the near stopper region. Any gravity effect on the pattern shape has been excluded as the patterns form equally in horizontal and vertical position of the cell. Therefore, the observed phenomenon (Fig. 1c-j) derives from the bulk motion brought on by electrical body forces lodged in the cloud, not forces on individual particles, as bulk motion of colloids cannot be explained solely by dipole–dipole interactions between particles.[28,29] The pattern dynamics is

driven by the interaction of the electrostatic body force and the ionic current. As the former stretches the cloud borders towards the electrodes, the later keeps pushing them out from the electrodes. Consequently, one can observe the slow, irregular motion of the formed spikes. This motion quits immediately when the field is interrupted. Then, the induced pattern looks like frozen from beginning and due to the thermal energy starts to dissipate very slowly. The original homogenous sample transparency (Fig. 1a) was achieved approximately in 3.5 hours of rest at room temperature. The pattern forming phenomenon was found to be reversible and independent on the field polarity. However, the electric field strength is a key parameter, as 3 kV/cm was critical for visually observable changes in the sample. Similar patterns were observed at 4 and 6 kV/cm. When applying the ac field with the strengths of 1–6 kV/cm, and frequencies of 1–500 Hz, no visual changes were observed. This fact points out the necessity of the space charge accumulation near the electrodes and the dc ionic current flowing through the sample.

The electric current density is determined by the space charge types and the corresponding charge carrier number densities in a given medium. In the studied TOFF, the space charge is represented by NH_4^+, OH^-, bound moisture, and other impurities[21]. The time dependent electric current $I(t)$ through the TOFF is shown in Figure 2. For 1 kV/cm and 2 kV/cm, the $I(t)$ curves resemble to a charging current. At the beginning the ions from the bulk volume are initiated to flow to the electrodes, where some of them can create electric double layers, changing so the contact potential difference. The decreasing current then reaches a certain level, whereby its continuity in electrode contacts is provided by electron transfer. At higher field strengths (3–6 kV/cm), the current fluctuations are more pronounced. The initial decrease is again associated with the charge settling response to the increased field strength. The further instabilities stem from the changes in the charge carrier mobility, not changes in the charge carrier concentration

due to ionization of the oil or emission from the electrodes which would appear in much higher field strengths. The decrease in the charge mobility is a result of the cloud formation. It is known that suspended particles impede ion flows and hence reduce the current.[29] This effect is more pronounced in the regions characterized by a strong particle interaction and aggregate formation. On the other hand, the interaction between the electric field and space charge gives rise to forces creating an eddy motion of the liquid. That motion irregularly releases the ion path in the concentrated particle regions, leading to the varying electric current.

The TOFF structure at nanoscale under the dc electric field was followed by SANS representing the scattered neutron intensity I as a function of the momentum transfer modulus q (Fig. 3). The SANS curve for the initial sample (zero electric field) corresponds to a typical system of polydisperse MNPs with the characteristic mean size of about 8 nm.[25,30] The high scattering contrast between magnetite and hydrogen-containing solvent allows one to neglect the scattering from the surfactant shell and magnetic neutron scattering from MNPs.[31] In Figure 3 an increase in the scattered intensity in the small q region emerges and intensifies with increasing field strength. This is a direct evidence for the particle aggregates in the TOFF induced by the above analyzed electrohydrodynamics and polarization forces between the particles. The dielectric contrast in the TOFF results in the induced electric dipole-dipole interactions and subsequent aggregation. Thus, the scattering curve obtained at 6 kV/cm represents two subsystems of scattering objects in the sample. The first, reflected in the intensity profile at $q > 0.1$ nm^{-1}, constitutes the non-aggregated particles, while the other involves the particle aggregates giving rise to the additional intensive scattering signal at $q < 0.1$ nm^{-1}. The lower estimate of the mean aggregate size can be determined from the minimal q covered in the experiment by $D \sim 2\pi/q$, yielding the value of about 300 nm. The rather sharp transition between

the particle and aggregate scattering indicates that only a small (below 1 %) fraction of all particles composes the aggregates. Thus, the main factor responsible for the increase in the scattering at small q-values is the growth of the aggregate volume with a V^2-effect on the scattered intensity. Furthermore, the residual surfactants do not aggregate in the applied field as examined by SANS on the pure surfactant (oleic acid) solution.

In ac electric fields of 1–6 kV/cm and frequencies of 1–500 Hz, the SANS curves coincide with that obtained in zero electric field. This corresponds to the visual observations when no patterns were induced by ac electric fields. Although the characteristic time of the particles' polarization is short enough to induce the dipole moments with the applied frequencies, there is apparently not enough time for mutual interactions between them. The polarization and repolarization takes place so fast that the induced dipoles cannot succeed in the attractive interaction. This is certainly dependent on the dielectric and rheological properties of the TOFF and its thermal energy. The time scans of SANS at 6 kV/cm and frequencies between 0 Hz and 1 Hz are depicted in Figure 4. One can deduce that the frequencies 50 mHz, 100 mHz, and 200 mHz allow the aggregate formation reflected in the small q intensity increase. At 500 mHz this signal still increases in time, but even after 60 minutes does not reach the level obtained in the dc field. It is significantly reduced at 800 mHz, and at 900 mHz the scattering curve fully coincides with the zero field curve. Consequently, the frequency of 800 mHz can be regarded as a critical frequency at which the applied electric field (6 kV/cm) induces the particle aggregation in the investigated TOFF.

The neutron scattering from the TOFF in zero electric field yields an isotropic 2D pattern (Fig. 5a) corresponding to the quasi-spherical MNPs. In the applied dc electric field 2D patterns become anisotropic (Fig. 5b) thus reflecting the elongated shape of the formed aggregates

oriented along the electric field. The latter is related to the 2D scattered intensity $I(\boldsymbol{q})$ proportional to the characteristic structure-factor of a chain-like aggregate, $S(\boldsymbol{q}) = [1 - \cos(\boldsymbol{q}\boldsymbol{e}\mu b)]/[1 - \cos(\boldsymbol{q}\boldsymbol{e}b)]$, where $\boldsymbol{e}$ is the unit vector along the chain, b is its cross-sectional diameter, and μ is the aggregate shape anisotropy. The $\boldsymbol{q}$-vector approximately lies in the 2D detector plain, and the scattering from chains oriented in a direction of that plain is determined by the radial angle φ between $\boldsymbol{q}$- and $\boldsymbol{e}$-vectors. Therefore, the aggregates aligned along the field direction ($\varphi = 0$) produce vertically extended 2D scattering patterns with maxima at φ equaled to $\pi/2$ and $3\pi/2$. When the aggregates are not fully oriented, the anisotropic pattern is a measure of the width of the orientation distribution around a preferable direction. The development of the scattering anisotropy with the electric field is shown in Fig. 5c by plotting the corresponding scattered intensities as a function of φ at a constant module of the scattering vector, q. At some combinations of b and μ, the structure-factor $S(\boldsymbol{q})$ can be approximated by $A(\boldsymbol{q}) + B(\boldsymbol{q})\sin^2\varphi$, where $A(\boldsymbol{q})$ and $B(\boldsymbol{q})$ are isotropic functions. This kind of approximation works well here. The corresponding fits (Fig. 5c) comprising just A and B parameters, which describe the intensity oscillations along φ, make it possible to estimate the anisotropy of the 2D intensity at a given q-value as $P = B/(A + B)$. As the scattering from the non-aggregated particles does not significantly vary with the field, the changes in Figure 5c are a direct consequence of the evolution of the aggregate structure and orientation. For the considered type of $S(\boldsymbol{q})$ the maximum in the φ-dependence is equal to μ^2, while the oscillation magnitude is determined by b. Figure 5c clearly demonstrates the increasing character of these two parameters with the increasing electric field. Hence, the development of the aggregation and orientation processes follows the electric field increase. These processes are far from saturation, as the anisotropy parameter P exhibits a continuous rise with the electric field strength (Fig. 5d). The anisotropy in the 2D scattering

patterns is observed in a restricted region. The largest one ($q < 0.04$ nm^{-1}) appeared at 6 kV/cm electric field strength. At higher q-values the P-parameter approaches zero following a transition to the scattering from isotropic structural units, i.e. non-aggregated particles.

Two factors restrict further comprehensive analysis of the observed anisotropy effect. First, the high polydispersity of the particles and aggregates extremely complicates the direct application of the structure-factor for modeling 2D scattering from the aggregate phase. Second, the aggregates are not fully oriented, meaning that one cannot determine the average longitude and cross-sectional size characteristics of the aggregates from the standard analysis of the cuts of the 2D scattered intensity parallel and perpendicular to the electric field direction.

In conclusion, we have demonstrated visually observable pattern formation in a transformer oil-based ferrofluid exposed to a dc electric field. The presence of space charge and its motion towards electric field gradients was assumed to be a trigger of the colloidal cloud formation. Electrical forces due to space charge and permittivity variation each play a role in inducing pattern formation and its dynamics. The electric field induced particle aggregation has been confirmed by *in situ* SANS experiments. Anisotropic structures have been observed in two dimensional scattering patterns. The pattern formation phenomenon can be exploited in preparation of patterned ferrofluid layers by solidification of the electrohydrodynamically driven structures. Electric field induced particle aggregation may be considered in theories describing the breakdown field strength of transformer oil-based ferrofluids.

ACKNOWLEDGMENT

This work is partially based upon experiments performed at the KWS-1 instrument operated by JCNS at the Heinz Maier-Leibnitz Zentrum (MLZ), Garching, Germany. The authors gratefully

acknowledge the financial support provided by NMI3 to perform the neutron scattering measurements at the Heinz Maier-Leibnitz Zentrum (MLZ), Garching, Germany. The work is also supported by Slovak Academy of Sciences and Ministry of Education in the framework of projects VEGA No. 2/0043/12, 2/0045/13, 1/0311/15, Ministry of Education Agency for structural funds of EU in frame of projects Nos. 26110230061, 26220120046, 26220120055 and 26220220182, Slovak Research and Development Agency in project APVV 0171-10, and COST RADIOMAG TD 1402. The authors thank Dr. Elena Alina Tăculescu (Moacă) for preparing the studied ferrofluid, and Andrey Churakov for the help in organization of the neutron experiments at IBR-2.

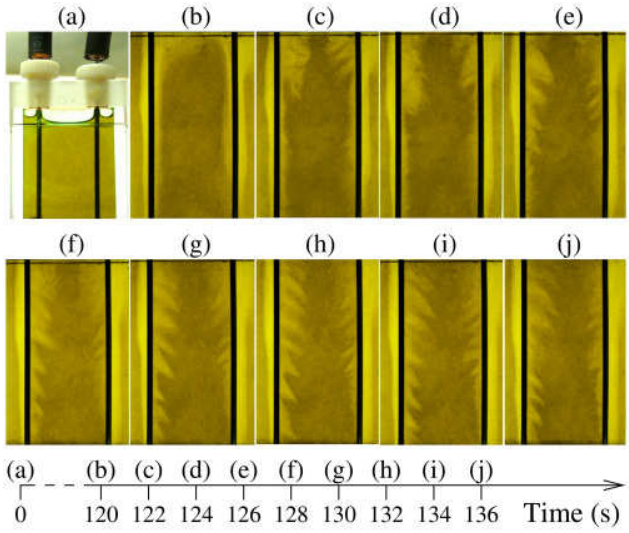

Figure 1. Transformer oil-based ferrofluid in zero electric field (a). Time evolution of electrohydrodynamically driven patterns in the sample exposed to the dc electric field of 5 kV/cm (b–j). The photographs are artificially colorized to enhance the contrast.

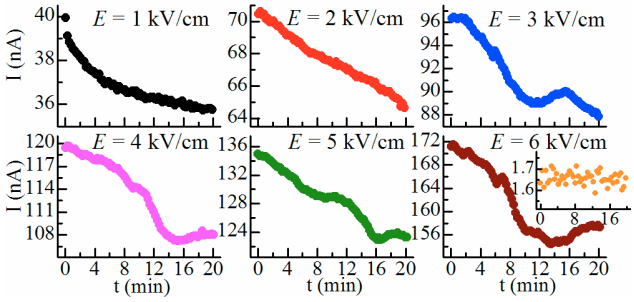

Figure 2. Time dependent dc electric current through the ferrofluid sample at different electric field strengths. The inset at 6 kV/cm shows the dc current through the transformer oil (base liquid) at this field.

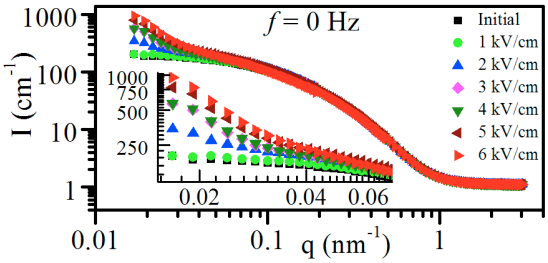

Figure 3. SANS curves for the ferrofluid exposed to the dc electric field strengths from 0 kV/cm (Initial) to 6 kV/cm.

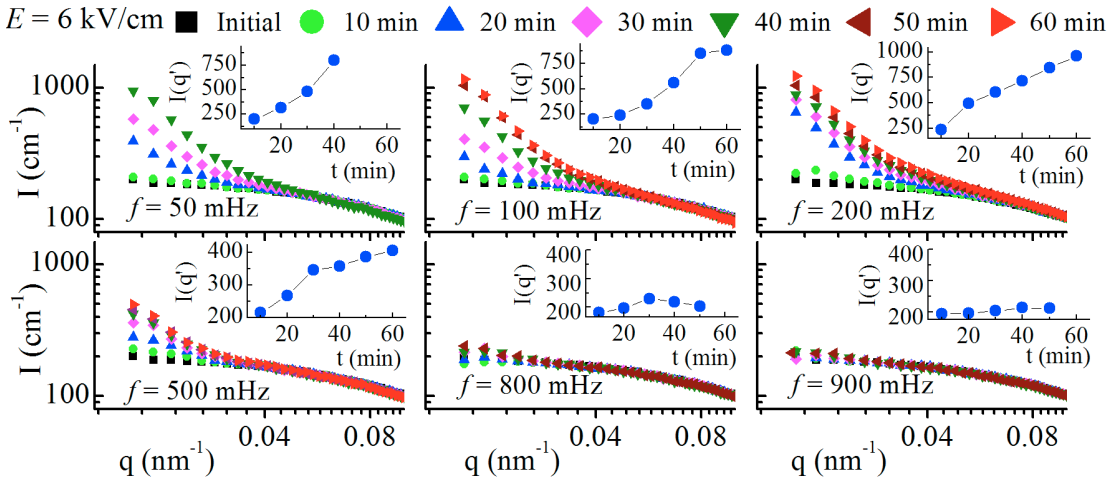

Figure 4 Time evolution of the SANS curves for the ferrofluid in ac electric fields (6 kV/cm) with frequencies between 0 and 1 Hz. Insets show the time variation of the characteristic intensity $I(q')$ taken at the vicinity of the minimal q-value covered ($q' = 0.019$ nm^{-1}). Following the clear effect and aiming to find the critical frequency, further time effects at 50, 800, and 900 mHz have not been measured.

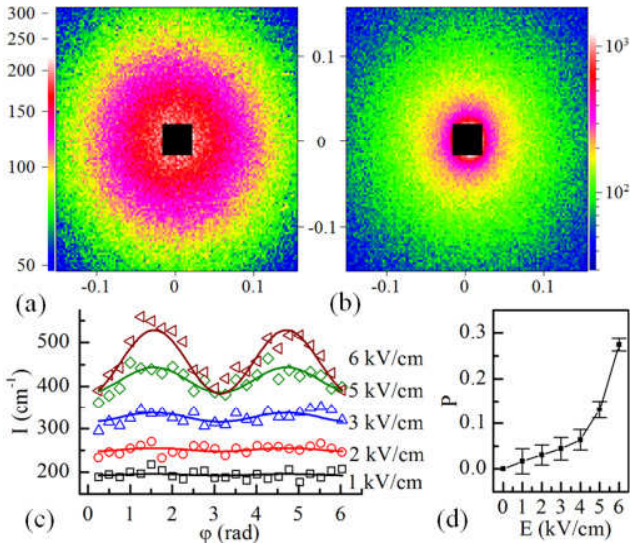

Figure 5. 2D scattering patterns for the ferrofluid in zero (a) and 6 kV/cm dc electric field (b). Both axes represent q (nm^{-1}). The scattered intensity dependent on the radial angle φ taken at q = 0.024 nm^{-1} for different electric field strengths (c). Solid lines show the fits by the model function $A + B \sin^2\varphi$. The cut at 4 kV/cm is omitted because of a partial overlap with the other data. The P-parameter of the scattering anisotropy as a function of the electric field strength (d).

REFERENCES

1 R. E. Rosensweig, Ferrohydrodynamics. Courier Dover Publications (1997).

2 A. Bitar, C. Kaewsaneha, M. M. Eissa, T. Jamshaid, P. Tangboriboonrat, D. Polpanich, and A. Elaissari, J. Colloid Sci. Biotechnol. 3, 1 (2014).

3 C. Scherer and A. M. Figueiredo Neto, Braz. J. Phys. 35, 3A (2005).

4 V. L.Aksenov, M. V. Avdeev, M. Balasoiu, D. Bica, L. Rosta, Gy. Torok, and L. Vekas, J. Magn. Magn. Mater.258–259 (2003).

5 T. Kruse, H.-G. Krauthäuser, A. Spanoudaki, and R. Pelster, Phys. Rev. B 67, 094206 (2003).

6 V. S. Mendelev and A. O. Ivanov, Phys. Rev. E 70, 051502 (2004).

7 A. Wiedenmann, U. Keiderling, K. Habicht, M. Russina, and R. Gähler, Phys. Rev. Lett. 97, 057202, (2006).

8 M. Klokkenburg, B. H. Erné, J. D. Meeldijk, A. Wiedenmann, A. V. Petukhov, R. P. A. Dullens, and A. P. Philipse, Phys. Rev. Lett. 97, 185702, (2006).

9 R. Rungsawang, J. da Silva, C.-P. Wu, E. Sivaniah, A. Ionescu, C. H. W. Barnes, and N. J. Darton, Phys. Rev. Lett. 104, 255703 (2010).

10 D. Heinrich, A. R. Goñi, A. Smessaert, S. H. L. Klapp, L. M. C. Cerioni, T. M. Osán, D. J. Pusiol, and C. Thomsen, Phys. Rev. Lett. 106, 208301 (2011).

11 F. Smallenburg, H. R. Vutukuri, A. Imhof, A. van Blaaderen, and M. Dijkstra, J. Phys. Condens. Matter, 24, 464113 (2012).

12 J. Lyklema, Curr. Opin. Colloid Interface Sci. 18, 2 (2013).

13 M. E. Leunissen, H. R. Vutukuri, and A. van Blaaderen, Adv. Mater. 21, 30 (2009).

14 M. Zrinyi, J. Electrost. 71, 3 (2013).

15 K. Barros and E. Luijten, Phys. Rev. Lett. 113, 017801 (2014).

16 I. Nkurikiyimfura, Y. Wang, and Z. Pan, Renew. Sustain. Energy Rev. 21 (2013).

17 V. Segal, A. Hjortsberg, A. Rabinovich, D. Nattrass, and K. Raj, in Conference Record of the 1998 IEEE International Symposium on Electrical Insulation (IEEE, Piscataway, NJ, 1998), Vol. 2, pp. 619–622.

18 J.-C. Lee, H.-S. Seo, and Y.-J. Kim, Int. J. Therm. Sci., 62, pp. 29–33 (2012).

19 J. Miao, M. Dong, M. Ren, X. Wu, L. Shen, and H. Wang, J. Appl. Phys. 113, 204103 (2013).

20 M. Rajnak, J. Kurimsky, B. Dolnik, K. Marton, L. Tomco, A. Taculescu, L. Vekas, J. Kovac, I. Vavra, J. Tothova, P. Kopcansky, and M. Timko, J. Appl. Phys. 114, 034313 (2013).

21 M. Rajnak, J. Kurimsky, B. Dolnik, P. Kopcansky, N. Tomasovicova, E. A. Taculescu-Moaca, and M. Timko, Phys. Rev. E 90, 032310 (2014).

22 J. G. Hwang, M. Zahn, F. M. O'Sullivan, L. A. A. Pettersson, O. Hjortstam, and R. Liu, J. Appl. Phys. 107, 1, pp. 014310–014310–17 (2010).

23 J. G. Hwang, M. Zahn, and L. A. A. Pettersson, J. Appl. Phys. 109, 084331 (2011).

24 D. Bica, L. Vékás, and M. Raşa, J. Magn. Magn. Mater. 252, pp. 10–12 (2002).

25 L. Vékás, M. V. Avdeev, and D. Bica, in NanoScience in Biomedicine, D. Shi, Ed. Berlin, Heidelberg: Springer Berlin Heidelberg, 2009, pp. 650–728.

26 A. I. Kuklin, A. K. Islamov, and V. I. Gordeliy, Neutron News 16, 16 (2005).

27 A. V. Feoktystov, H. Frielinghaus, Z. Di, S. Jaksch, V. Pipich, M.-S. Appavou, E. Babcock, R. Hanslik, R. Engels, G. Kemmerling, H. Kleines, A. Ioffe, D. Richter, and T. Brückel, J. Appl. Crystallogr. 48, 1, pp. 61–70, (2015).

28 M. Trau, S. Sankaran, D. A. Saville, and I. A. Aksay, Nature, 374, 6521, pp. 437–439 (1995).

29 M. Trau, S. Sankaran, D. A. Saville, and I. A. Aksay, Langmuir, 11, 12, pp. 4665–4672, (1995).

30 M.V.Avdeev, V.L.Aksenov, Physics Uspekhi, 53, 10, pp. 971–993 (2010).

31 M. V. Avdeev, D. Bica, L. Vékás, V. L. Aksenov, A. V. Feoktystov, O. Marinica, L. Rosta, V. M. Garamus, and R. Willumeit, J. Colloid Interface Sci. 334, 1, pp. 37–41, (2009).